Electronic Supplementary Material (ESI) for ChemComm.
This journal is © The Royal Society of Chemistry 2019

Supporting Information

Selective Electroreduction of Dinitrogen to Ammonia on Molecular Iron Phthalocyanine /O-MWCNT Catalyst under Ambient Conditions

Fanfan Xu, [a#] Linlin Zhang, [a#] Xin Ding, [a,b]* Meiyu Cong, [a] Yu Jin, [b] Lin Chen, [c] Yan Gao[b]*

[a] College of Chemistry and Chemical Engineering, Qingdao University, Qingdao 266071, Shandong, (PR China)
[b] State Key Laboratory of Fine Chemicals, Dalian University of Technology (DUT), Dalian 116024, Liaoning, (PR China)
[c] State Key Laboratory of Environment-friendly Energy Materials, Southwest University of Science and Techaology, Sichuan 621010 (PR China)
[#] These authors contribute equally to the article

*Corresponding author: *dingxin@qdu.edu.cn; dr.gaoyan@dlut.edu.cn*

Experimental Procedures

Materials

All the reagents were used as received without further purification. Iron (II) Phthalocyanine, $Na_2[Fe(NO)(CN)_5]$ and p-$C_9H_{11}NO$ were purchased from Sigma-Aldrich Chemical Reagent Corporation. N_2 gas (99.999%) and Ar gas (99.999%) were purchased from Dalian Special Gases Corporation. O-MWCNT was purchased from Nanjing XFNANO Materials Technology Corporation. The carbon paper (CP) was purchased from Toray Industries in Japan. The deionized water used throughout all experiments was purified through a Millipore system. $^{15}N_2$ gas was purchased from Shanghai Engineering Research Center of Stable Isopotc.

Preparation of FePc/O-MWCNT electrode

30 mg of O-MWCNTs were dispersed in 30 ml of DMF with the assistance of sonication for 1 h. Then, a calculated amount of FePc dissolved in DMF was added to the O-MWCNT suspension followed by 30 min of sonication to obtain a well-mixed suspension. The mixed suspension was further stirred at room temperature for 20 h. Subsequently, the mixture was centrifuged and the precipitate was washed with DMF for three times and ethanol twice. Finally, the precipitate was vacuum dried to yield the final FePc/O-MWCNT.

12 mg FePc/O-MWCNT was suspended in 1200 μL Nafion solution with ultrasonically for 1 h to produce the homogeneous catalyst ink. Then, 10 μL of ink was coated on carbon paper (CP, $2\times0.5\ cm^2$), which will be dried at room temperature.

Characterizations

XRD data were obtained from a Shimazu XRD-6100 diffractometer with Cu Kα radiation (40 kV, 30 mA) of wavelength 0.154 nm (Japan). The position of the C1s peak, that is 284.4 eV, was used to correct the binding energies of all the catalysts. The morphology and microstructure of the samples were investigated by Field-Emission Scanning Electron Microscopy (FESEM, ULTRA Plus, Zeiss). SEM measurements were carried out on a XL30 ESEM FEG scanning electron microscope at an accelerating voltage of 20 kV. Transmission electron microscopy (TEM, TECNAI G2 F20 STWIN D2278, FEI) and high-resolution TEM (HRTEM) were carried out on microscope operated at an accelerating voltage of 200 kV. XPS measurements were performed on an ESCALABMK II X-ray photoelectron spectrometer with the exciting source of Mg. UV-Vis absorption spectra were recorded on a UV-Vis spectrophotometer (Shimadazu, UV-1800). Raman spectrum was collected on Renishaw with a 532 nm laser.

Electrochemical measurements

The electrochemical experiments were carried out in a two-channel electrolytic cell under ambient conditions, which was separated by perfluorosulfonic acid proton exchange membrane. The membrane was pretreated in H_2O_2 (5%) aqueous solution, and in ultrapure water at 80 ^oC for 1 h. And then, the membrane was dipped into 1 M H_2SO_4 for 1 h at 80 ^oC and finally boiled in water for 2 h. Electrochemical measurements were operated in a standard three-electrode system by a CHI660E electrochemical analyzer using Ag/AgCl as reference electrode, and graphite plate was used as the counter electrode and FePc/O-MWCNT/CP (2 ×0.5 cm^2) as working electrode respectively. Before the NRR experiment, the HCl electrolyte (0.1 M, pH = 1) would be pretreated to remove the dissolved gas, and then bubbled with N_2 for 35 min. All potentials were measured against an Ag/AgCl reference electrode and converted to the RHE reference scale using the equation: $E \text{ (vs. RHE)} = E \text{ (vs. Ag/AgCl)} + 0.224 \text{ V} + 0.0596 \times \text{pH}$, and all experiments were carried out at room temperature (25 °C).

The electrochemical activities of samples were examined by linear sweep voltammetry (LSV) with a scan rate of 5 mV/s at room temperature. The electrochemical impedance spectroscopy (EIS) measurements of samples were performed out in the same configuration from 10^5 to 0.01 Hz with an AC voltage of 5mV with electrochemical workstation. Cyclic Voltammetry (CV) taken at various scan rates (30, 60, 90, 120 and 150 mV/s) were recorded in the non-faradic potential range of 0.96-1.23 V vs. RHE (non-faradaic region) and were used to estimate the double-layer capacitance (C_{dl}). C_{dl} was determined as the linear slope by plotting anodic current density at 1.1 V against the scan rate. $C_{dl} = i_c/\nu$, where i_c represents the charging current, ν is the scan rate.

Determination of ammonia and hydrazine hydrate

The content of ammonia in the electrolyte after the reaction was measured by the indophenol blue method with some modification. 2 mL aliquot of the electrolyte was removed to color comparison tube, and add 2 mL 1 M NaOH solution containing salicylic acid and sodium citrate,1 mL of 0.05 M NaClO and 0.2 mL of 1 wt % sodium nitroferricyanide ($Na_2[Fe(NO)(CN)_5]$) , standing at room temperature for 2 h, and then to measuring the UV-Vis absorption spectrum of the solution.

The hydrazine present in the electrolyte was estimated by the method of Watt and Chrisp. A mixture of para-(dimethylamino) benzaldehyde (5.99 g), HCl (concentrated, 30 mL) and ethanol (300 mL) was used as a color reagent. First, preparing a series of reference solutions, by pipetting suitable volumes of the hydrazine hydrate-nitrogen 0.1 M HCl solution in colorimetric tubes. Second, making up to 5 mL with diluted hydrochloric acid electrolyte (pH = 1). Third, adding

5 mL above prepared color reagent and stirring 10 min at room temperature. Fourth, the absorbance of the resulting solution was measured at 455 nm, and the yields of hydrazine were estimated from a standard curve using 5 mL electrolyte and 5 mL color reagent.

Calculations

1. The rate of ammonia formation

The rate of ammonia formation was calculated as equation S1, where cNH_3 was the quality of concentration , V was the volume of the HCl electrolyte, t was the reduction reaction time, and m was the mass of catalysts. The total amount of NH_3 produced was measured using colorimetric methods and Ion chromatography.

$$r_{(NH_3)} = \frac{c_{(NH_3)} \times V}{t \times m_{cat.}} \qquad (S1)$$

Where:

$r_{(NH_3)}$: is ammonia formation rate in μg h^{-1} $mg^{-1}_{cat.}$.

$C_{(NH_3)}$: is ammonia concentration in the electrolyte in μg mL^{-1}.

V: is the volume of electrolyte in mL.

2. Faradaic efficiency (FE)

The faradaic efficiency was calculated as equation S2, where Q was the total charge passed through the electrobath, n (NH_3) was the total amount of ammonia produced. Assuming three electrons were needed to produce one NH_3 molecule.

$$FE_{NH_3}(\%) = \frac{F \times 3n_{(NH_3)}}{Q} \times 100\% \qquad (S2)$$

Where:

F: Faraday constant (96485 C mol^{-1}).

$n_{(NH_3)}$: is the amount of ammonia produced in μmol.

Q: is the total charge in C.

3. Turnover numbers (TON)

The turnover numbers were calculated as equation S3, where $n_{cat.}$ was the total loading amount of catalysts.

$$TON = \frac{n_{(NH_3)}}{n_{cat.}} \qquad (S3)$$

Where:

$n_{(cat.)}$:is the total amount of catalysts in μmol.

The Experiments of the ^{15}N Isotopic

The ^{15}N isotopic labeled experiment were performed using the $^{15}N_2$ isotope with the ^{15}N (99.99%) to certify the nitrogen origination of ammonia . Before the electrochemical reduction procedure, the electrolyte of 30 mL was saturated with $^{15}N_2$ for 30 min . After 2 h electrolysis at potential of -0.3 V (vs. RHE), the obtained electrolyte was then concentrated in a decompression distillation plant. The analysis of $^{15}NH_3$ product was conducted by the ^1H NMR with d^6-DMSO.

Theoretical Method

All of the quantum chemical computations were performed at the M06-2X/Def2-TZVP level of theory, by using the Gaussian 16 program (Revision B01). [1-3] The bond order analysis were carried out using the Mayer's scheme [4] by the Multiwfn program (3.6 version). [5] The Gibbs free energy change (ΔG) of every elemental coupled proton and electron transfer (CPET) step of the NRR process ($N_2 + 6H+ + 6e^- \rightarrow 2NH_3$) was calculated according to previous theoretical works. [6,7]

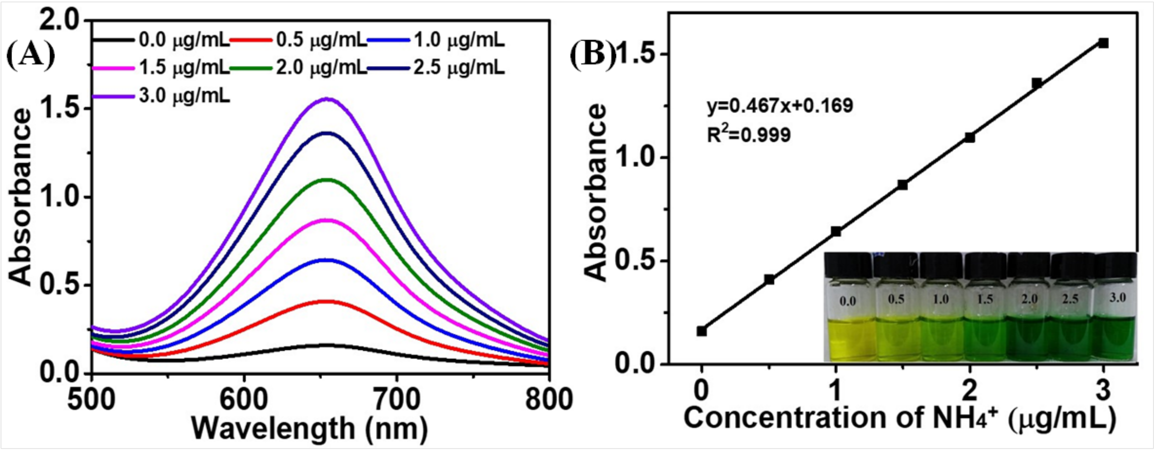

Fig. S1. (A) UV-Vis absorption spectra of indophenol assays with different NH_3 concentrations after incubated for 2 h at room temperature. (B) Calibration curve used for calculation of NH_3 concentrations.

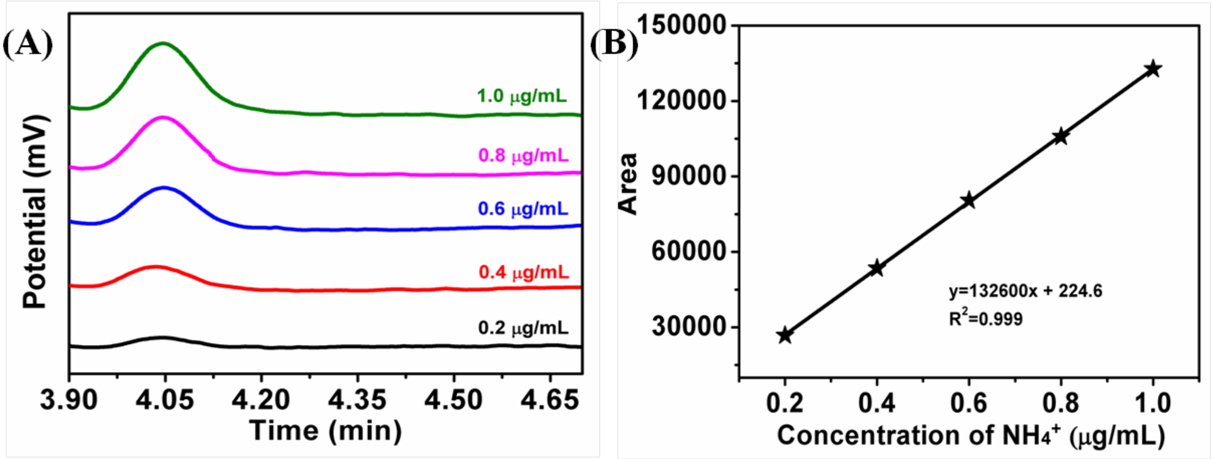

Fig. S2. (A) The determination of Ion chromatography with different NH_3 concentration. (B) Calibration curve used for calculation of NH_3 concentrations.

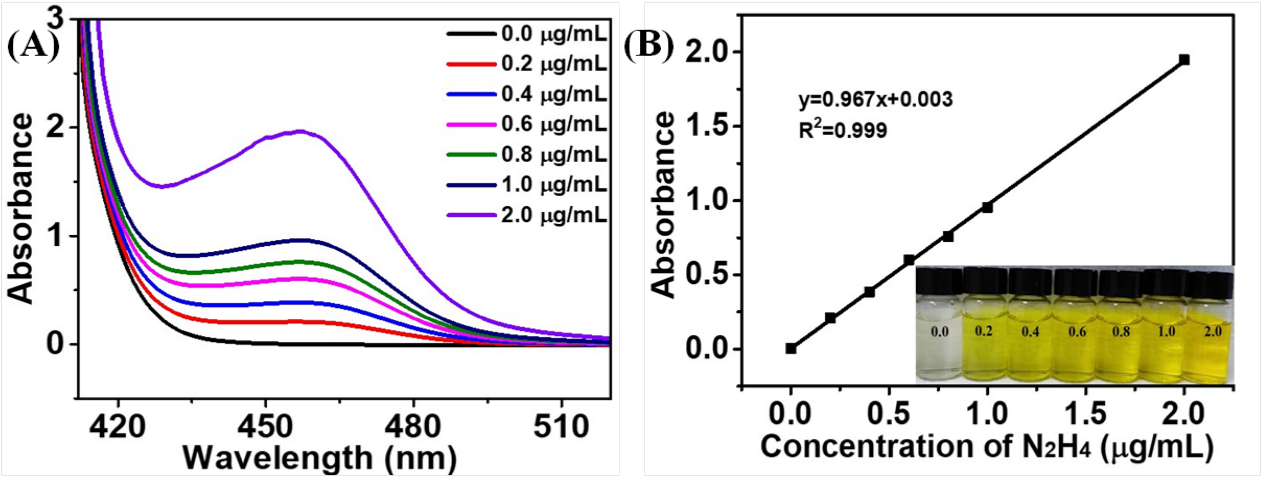

Fig. S3. (A) UV-Vis absorption spectra of various N_2H_4 concentrations after incubated for 10 min at room temperature. (B) Calibration curve used for calculation of N_2H_4 concentrations.

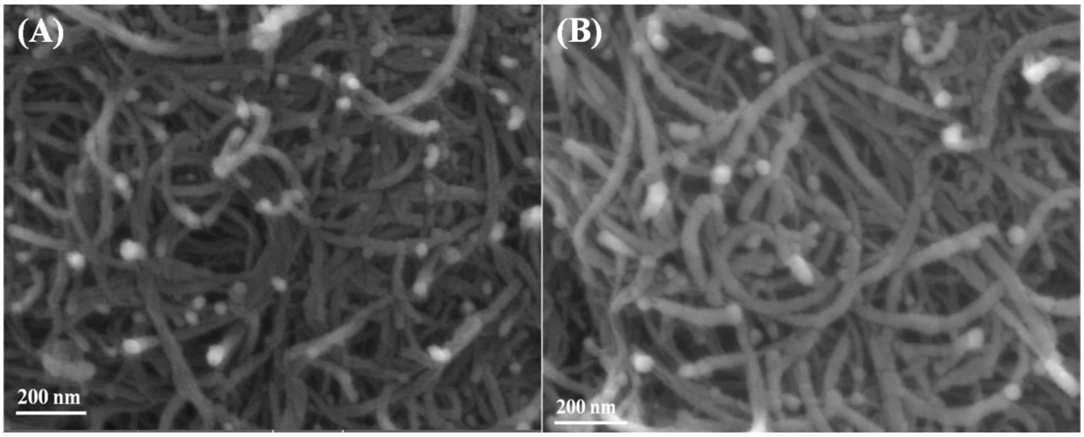

Fig. S4. SEM images of O-MWCNT (A) and the FePc/O-MWCNT catalysts (B).

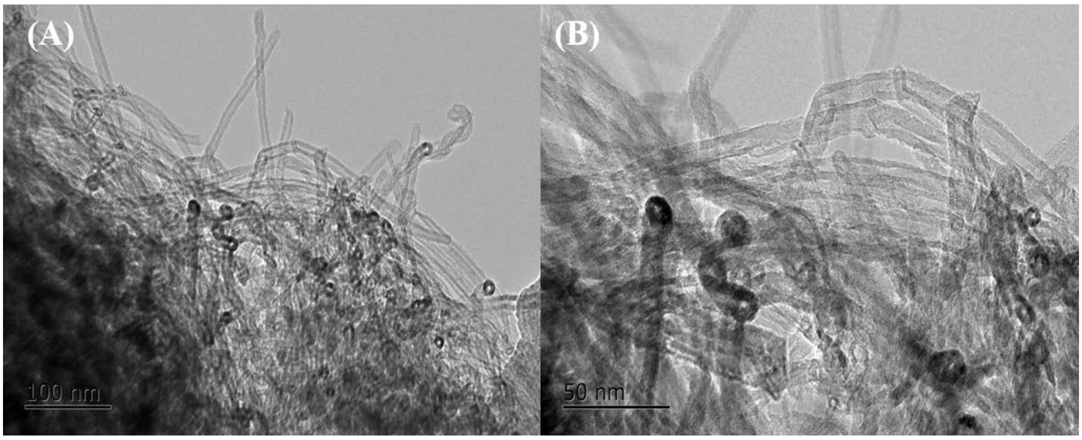

Fig. S5. HRTEM images of FePc/O-MWCNT.

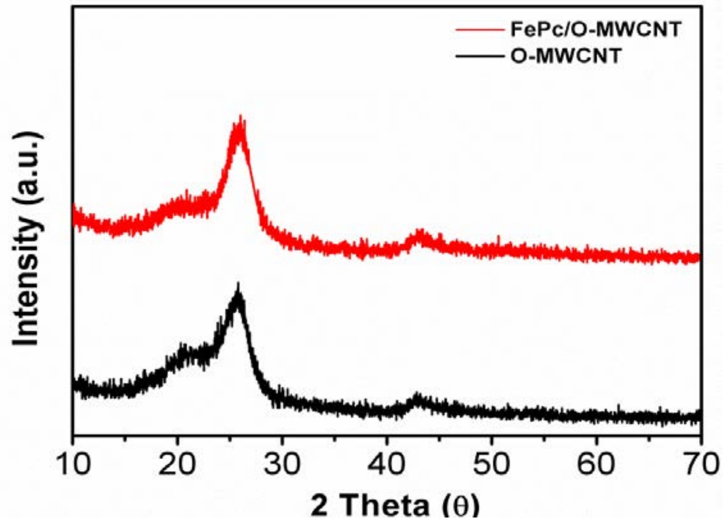

Fig. S6. XRD patterns of O-MWCNT and FePc/O-MWCNT.

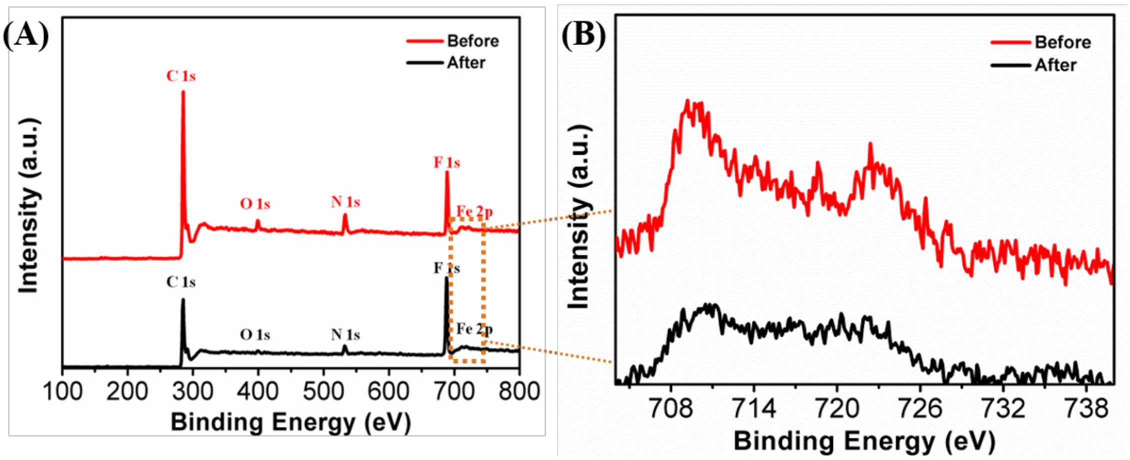

Fig. S7. XPS date of FePc/O-MWCNT before and after five cycles test.

The XPS date of before and after five cycles test was also carried out as shown in figure S7. The decrease in the loading of FePc could be found obvious in the XPS dates.

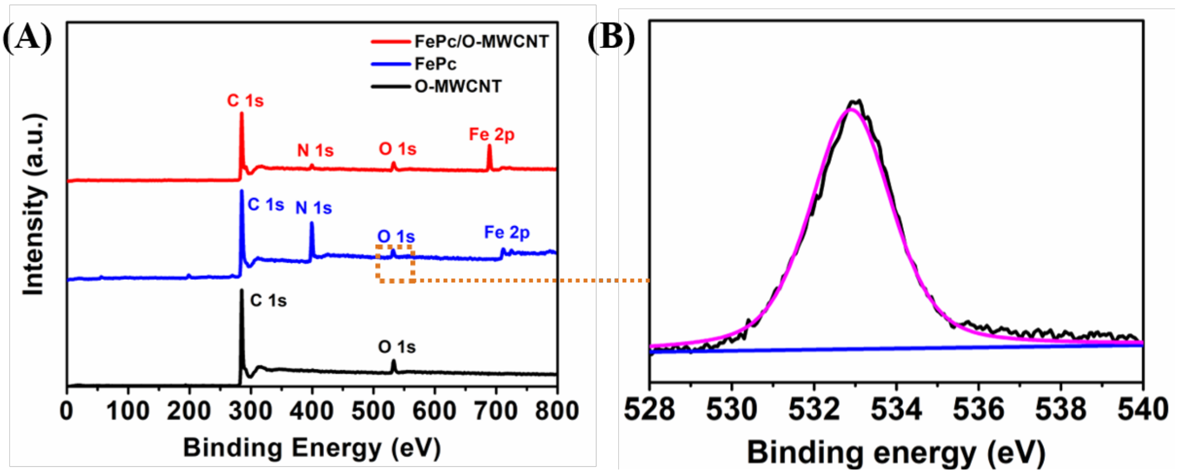

Fig. S8. (A) XPS patterns of the catalyst and raw materials; (B) The survey O 1s XPS spectra of FePc.

The peak observed in the O 1s XPS patterns at *ca.*533 eV was ascribed to adsorbed oxygen.

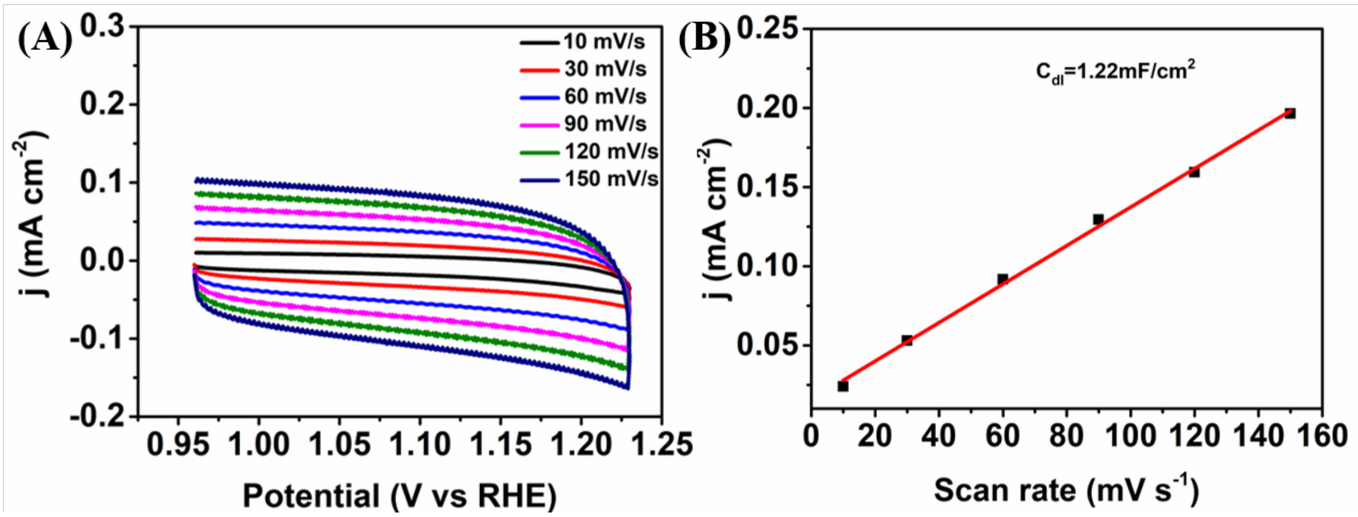

Fig.S9. (A) Cyclic Voltammograms for synthesized FePc/O-MWCNT at various scan rates; (B) charging current density, plotted against scan rates the double layer capacitance (C_{dl}).

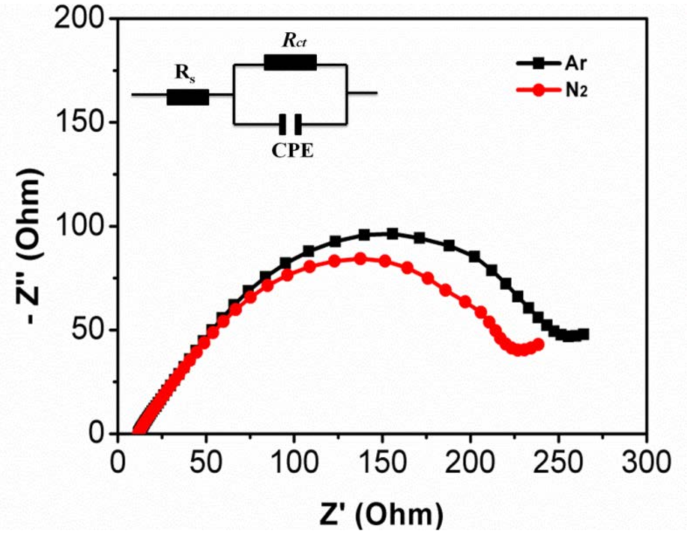

Fig.S10. The electrochemical impedance measurements of the FePc/O-MWCNT in N_2 and Ar saturated electrolytes.

Electrochemical impedance spectroscopy was also used to investigate the kinetics of FePc/O-MWCNT. Nyquist plots were fitted with an equivalent circuit as demonstrated in the inset of Figure S10. We assigned R_{ct} as the charge transfer resistance at the interface between the catalyst and the electrolyte, which generally represents the electrochemical activity of the electrode. EIS curves show that FePc/O-MWCNT delivers smaller impedance in N_2 saturated electrolyte than that in Ar under the potential of -0.3 V. So, NRR occurred on FePc/O-MWCNT catalyst.

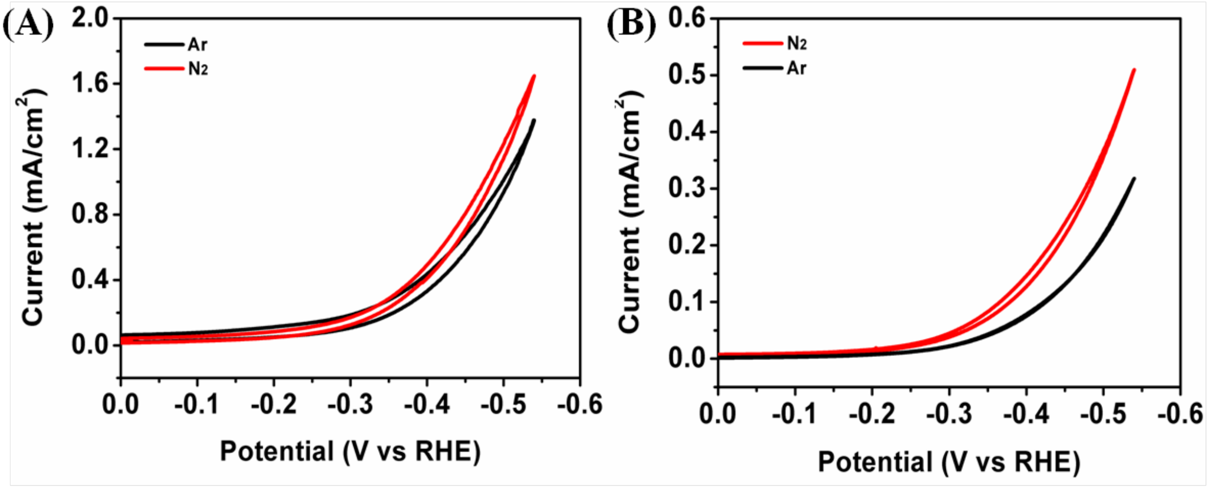

Fig.S11. The Cyclic voltammograms data of the FePc/O-MWCNT (A) and FePc (B) in Ar and N_2 Ar saturated electrolytes.

The CV for both FePc and FePc/o-MWCNT in Ar and N_2 saturated electrolytes had been carried out as shown in figure S11. The current density increased obviously from an Ar saturated to N_2 saturated electrolyte. Combining the comparison in figure S20, we confirmed NRR occurred on FePc. And the FePc acted as the catalytic center in the FePc/O-MWCNT, while the O-MWCNT greatly improved the recyclability of the molecular.

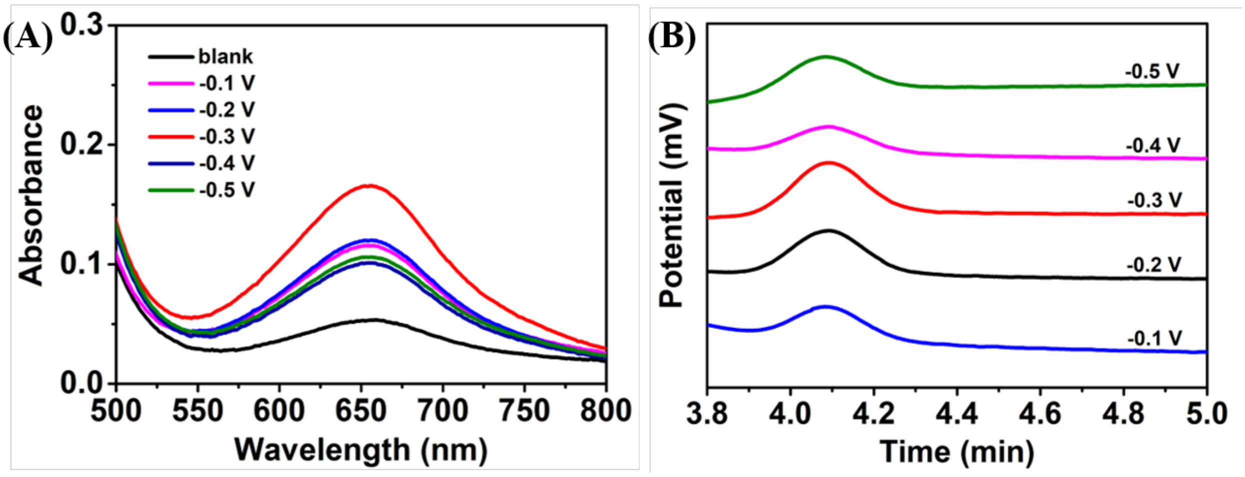

Fig. S12. (A) The yield rate of NH^{4+} formation and corresponding UV-Vis absorption spectra of the FePc/O-MWCNT at -0.1 V to -0.5 V; (B) The determination of Ion chromatograms of the FePc/O-MWCNT at -0.1 V to -0.5 V.

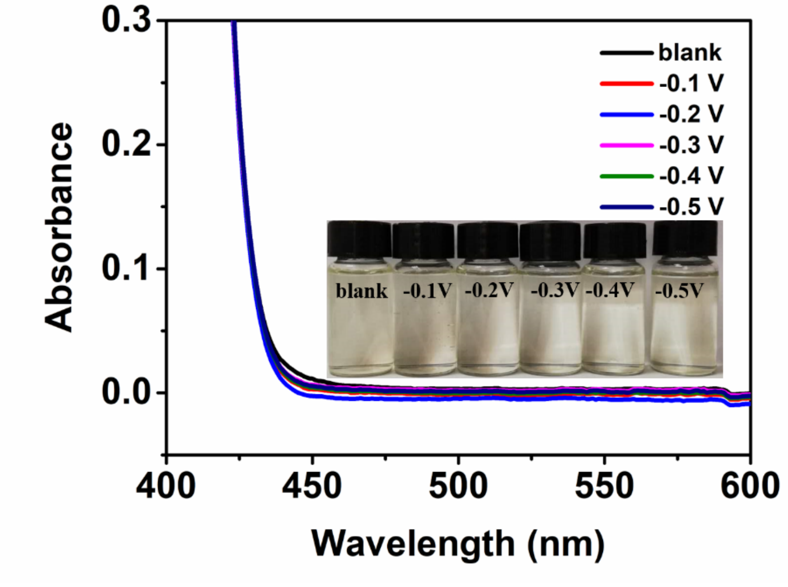

Fig. S13. The yield rate of $N_2H_4{\cdot}H_2O$ formation and corresponding UV-vis absorption spectra at -0.1 V to -0.5 V.

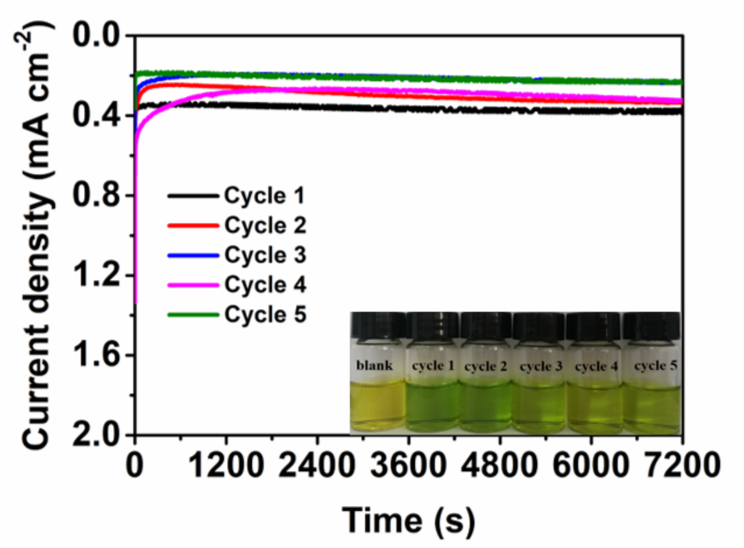

Fig. S14. The current density over time during cycling tests of FePc/O-MWCNT.

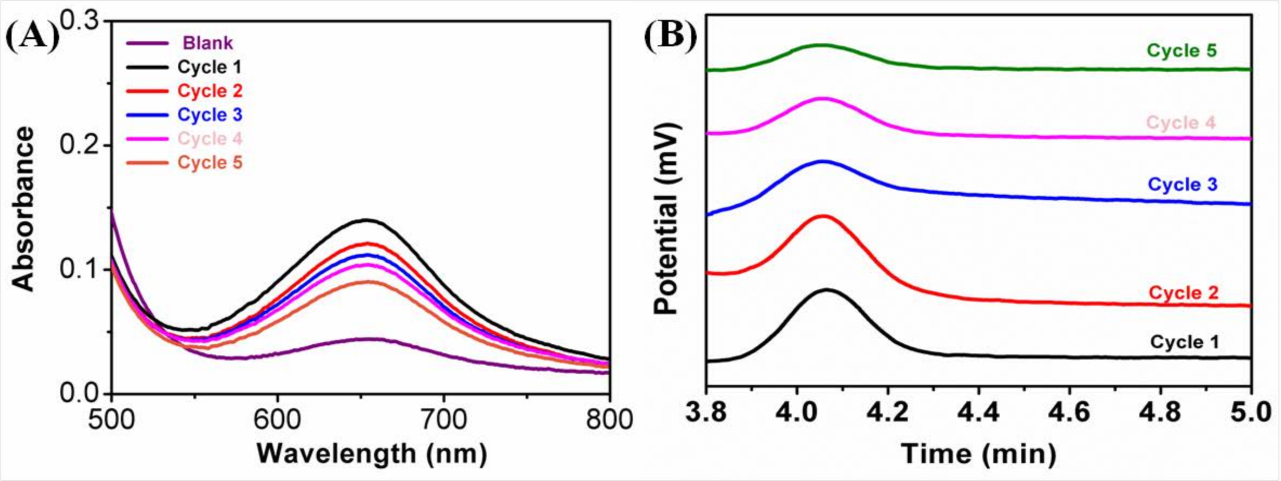

Fig. S15. (A) Stability of the UV-Vis absorption spectra at the potential of -0.3 V vs. RHE using the FePc/O-MWCNT catalysts; (B) Stability of the Ion chromatograms at the potential of -0.3 V vs. RHE using the FePc/O-MWCNT catalysts.

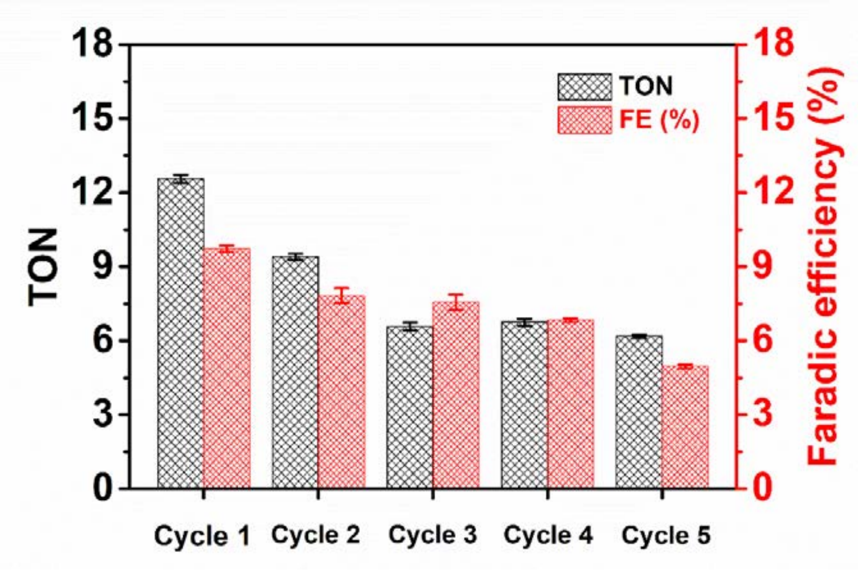

Fig. S16. TON and FE obtained from cycling tests of FePc/O-MWCNT.

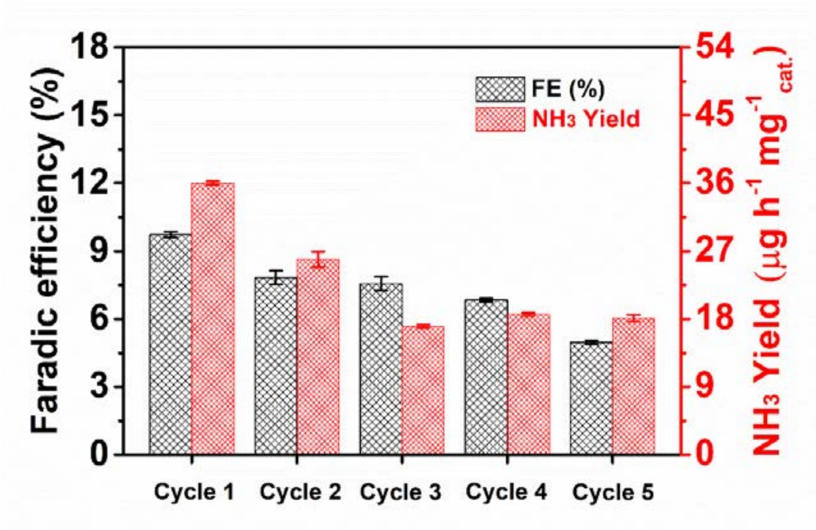

Fig. S17. FE and NH_3 Yield of FePc/O-MWCNT catalyst during five consecutive cycles at the potential of -0.3 V.

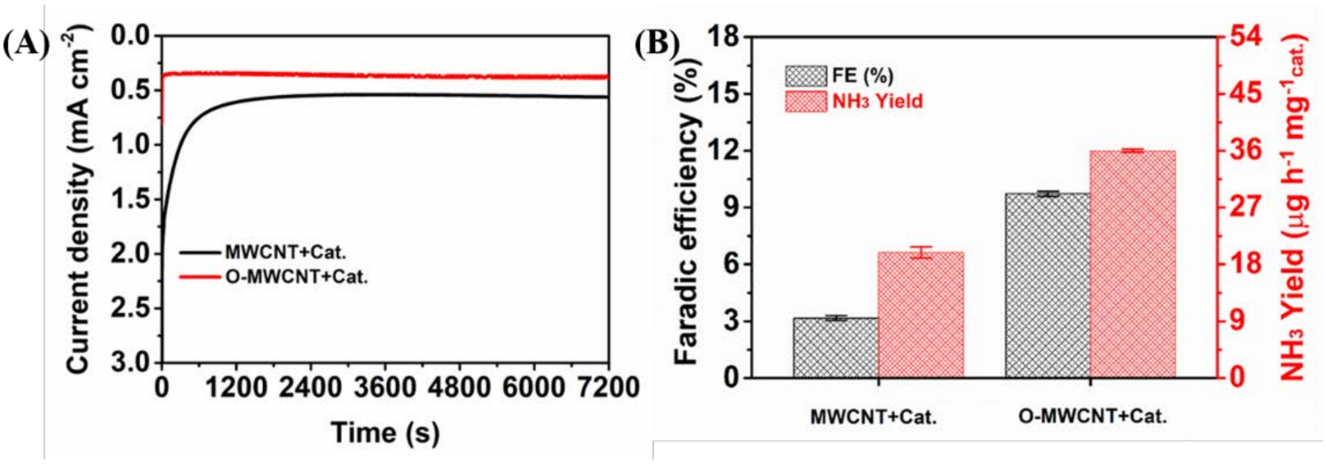

Fig. S18. (A)The current density over time using FePc/O-MWCNT and FePc/MWCNT for the NRR at an applied potential of -0.3 V vs. RHE; (B) FE and yield values obtained from FePc/MWCNT and FePc/O-MWCNT.

A comparison between MWCNT and O-MWCNT had also been carried out as shown in figure S18. The FePc/O-MWCNT displayed superior performance than FePc/MWCNT in FE and NH_3 yield, but lower in current density. The hydroxyl on O-MWCNT played a positive effect on electrocatalytic NRR.

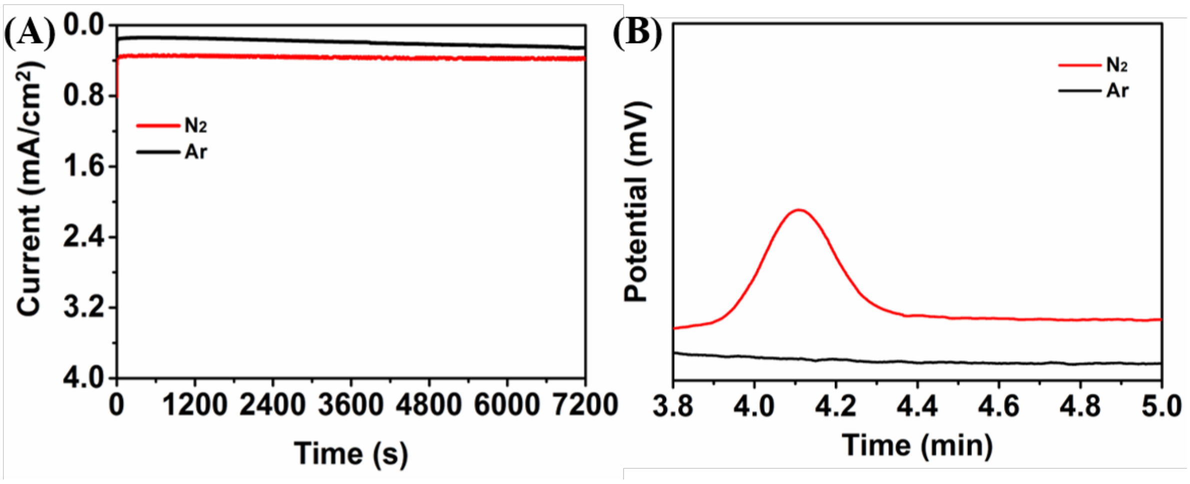

Fig. S19. (A)The dependence of current density on the time using FePc/O-MWCNT in the Ar, N_2 saturated electrolyte for NRR at applied potentials of -0.3 V vs. RHE; (B) Ion chromatogram for the electrolytes of FePc/O-MWCNT in the Ar, N_2 saturated after electrolysis for 2 h.

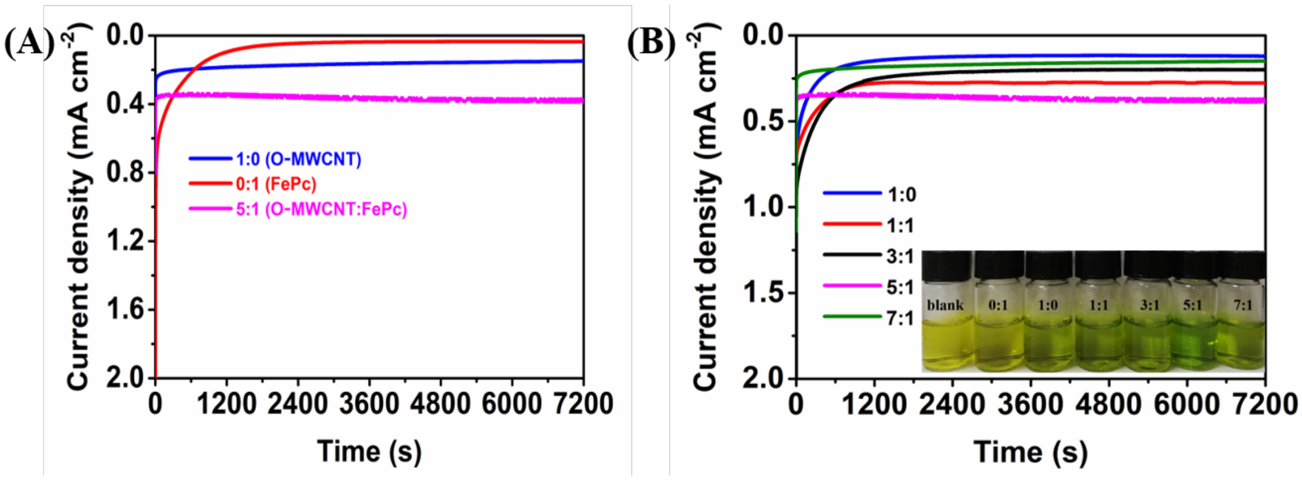

Fig. S20. (A)The current density over time using FePc, O-MWCNT and FePc/O-MWCNT for the NRR at an applied potential of -0.3 V vs. RHE; (B) The current density over time using FePc/O-MWCNT with various mass ratios for the NRR.

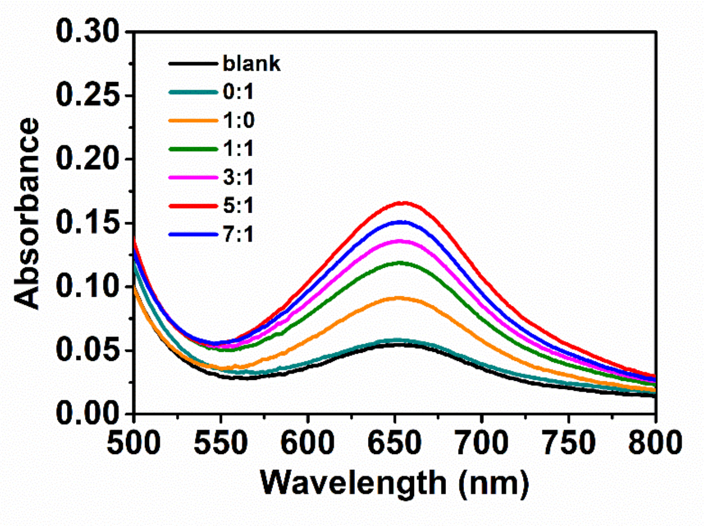

Fig. S21. UV-Vis absorption spectra of the electrolyte with different ratios FePc/O-MWCNT as electrocatalyst under the potential of -0.3 V vs. RHE.

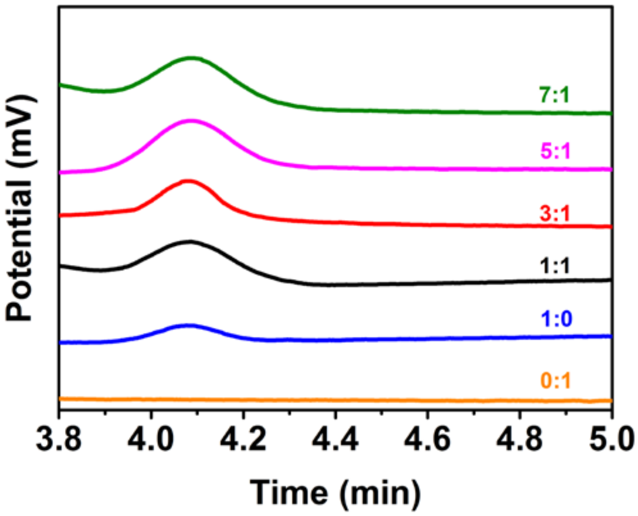

Fig. S22. Ion chromatograms obtained from the electrolytes following reactions over FePc/O-MWCNT with various mass ratios after electrolysis for 2 h.

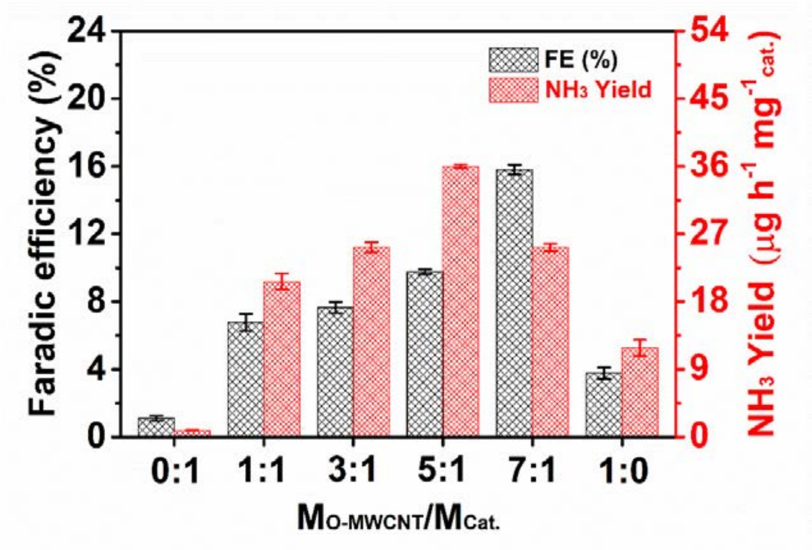

Fig. S23. The FE and yield values for NH_3 production over FePc/O-MWCNT with various mass ratios.

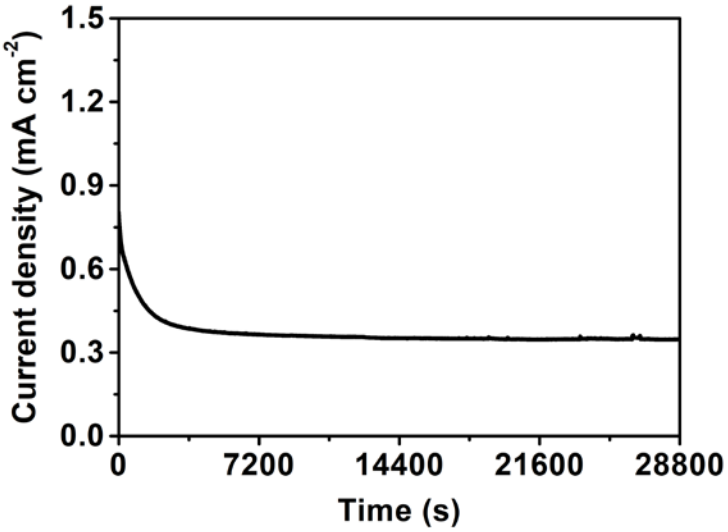

Fig. S24. The stability of the FePc/O-MWCNT during 8h operation.

Stability is an important property for NRR catalyst, the durability of the FePc/O-MWCNT was also investigated. After five cycles, the TON was decreased from 12.56 to 6.18 and the FE from 9.73% to 4.97% as shown in Figures S16. While, in the long-time stability tests, the current density remained at *ca*. 0.3 mA/cm^2 with a slight decrease over this duration. This phenomenon should be coursed by the increased contribution of the NRR-inactive O-MWCNT during the catalytic period.

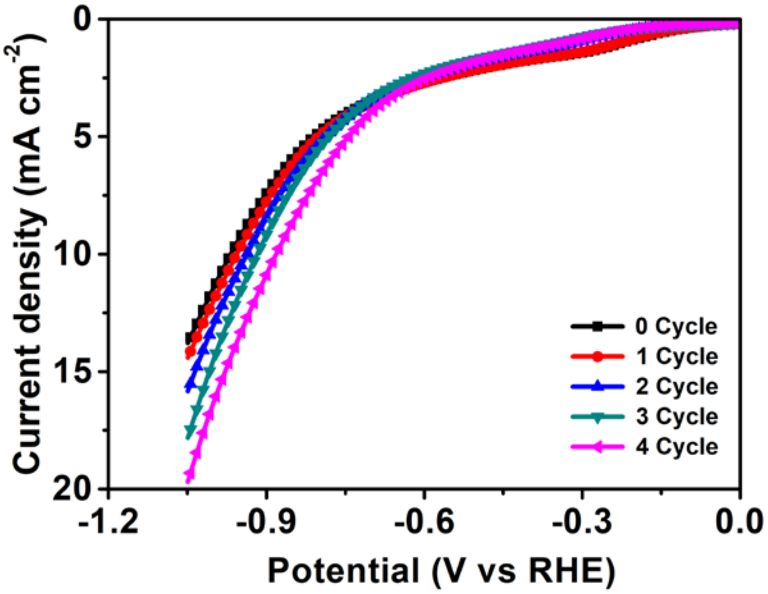

Fig. S25. LSV curves for FePc/O-MWCNT after cycling tests for NRR.

After five cycles, the TON was decreased from 12.56 to 6.18 and the FE from 9.73% to 4.97%, indicating possible loss or degradation of the FePc. The NRR performance was also carried out from linear sweep voltammetry (LSV) measurements to confirm the possible loss or degradation of the FePc.

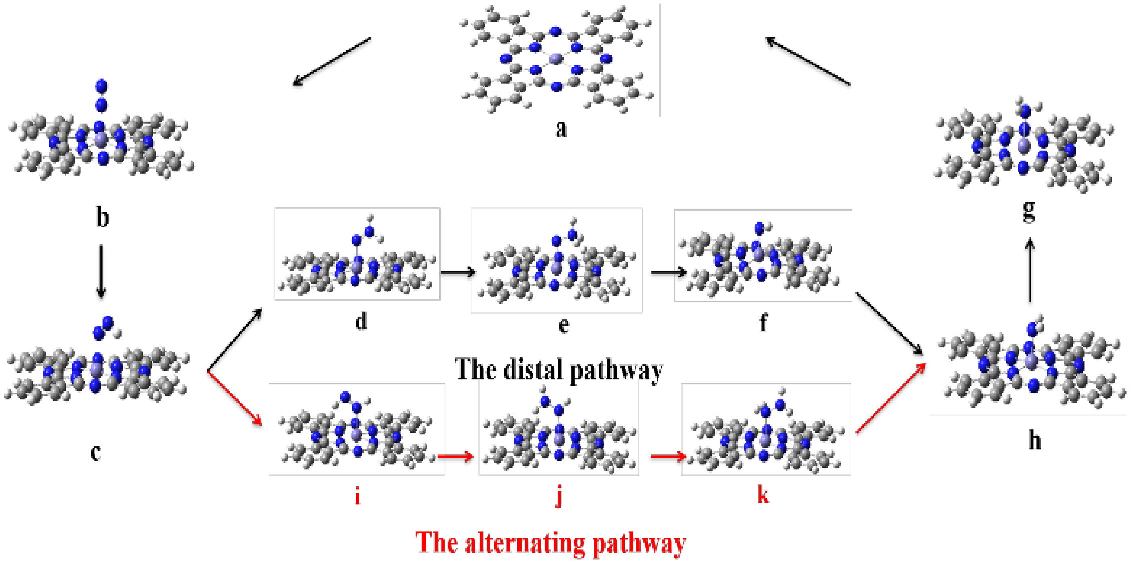

Fig. S26. The pathway for NRR on FePc catalyst.

Table S1 The bond distance of Fe-N in the catalytic period of NRR on FePc

The Distal Path	**Bond distance of Fe-N (angstrom)**	**The Alternating Path**	**Bond distance of Fe-N (angstrom)**
Fe-NN*	2.014	Fe-NN*	2.014
Fe-NNH*	2.127	Fe-NNH*	2.127
Fe-NNH$_2$*	**1.934**	**Fe-NHNH***	**1.980**
Fe-NNH$_3$*	**1.976**	**Fe-NHNH$_2$***	**2.084**
Fe-NH*	**1.621**	**Fe-NH$_2$NH$_2$***	**2.060**
Fe-NH$_2$*	1.828	Fe-NH$_2$*	1.828
Fe-NH$_3$	2.062	Fe-NH$_3$	2.062

Table S2 A representative summary of electrocatalysts previously reported for NRR

Catalyst	FE (%)	NH$_3$ Yield	Electrolyte	Potential (V vs RHE)	Reference
Au@ TiO$_2$	8.11%	21.4 μg h^{-1} mg$^{-1}_{\text{cat.}}$	0.1M HCl	-0.2 V	Adv. Mater. 2017, 29, 1606550
Amorphous phase Bi$_4$V$_2$O$_{11}$/CeO$_2$	10.16 %	23.21 μg h^{-1} mg$^{-1}_{\text{cat.}}$	0.1M HCl	-0.2 V	Angew Chem. 2018, 21, 6181–6184
Nb$_2$O$_5$ nanofiber	9.26 %	43.6 μg h^{-1} mg$^{-1}_{\text{cat.}}$	0.1M HCl	-0.55 V	Nano Energy 2018,52, 264–270
FeN$_4$	10.50 %	137.95 μg h^{-1} mg$^{-1}_{\text{FePc}}$	0.1M Na$_2$SO$_4$	-0.3 V	ACS Catal. 2019, 9, 7311−7317
BP NSs	5.07 %	31.37 μg h^{-1} mg$^{-1}_{\text{cat.}}$ (at - 0.7 V)	0.01 M HCl	-0.6 V	Angew Chem. 10.1002/ange.201813174
VN	6.0 %	3.3×10^{-10} mol s^{-1} cm^{-2}	0.05 M H$_2$SO$_4$	-0.1 V	J. Am. Chem. Soc. 2018, 140, 13387−13391
N, P co-doped hierarchical porous carbon	4.2 %	0.97 μg h^{-1} mg$^{-1}_{\text{cat.}}$	0.1 M HCl	-0.2 V	Chem. Commun., 2019,55, 687-690
Fe$_3$S$_4$	6.45 %	75.4 μg h^{-1}mg$^{-1}_{\text{cat.}}$	0.1M HCl	-0.4 V	Chem. Commun., 2018,54, 13010-13013
Single Mo atom	6.8 ± 0.3 %	31.5±1.2μg h^{-1} mg$^{-1}_{\text{cat.}}$	0.1 M HCl	-0.25 V	Angew. Chem. 10.1002/ange.201811728
AuSAs-NDPCs	12.3 %	2.32 μg h^{-1} cm^{-2}	0.1 M HCl	-0.2 V	Small Methods 2018, 2, 1800202
Ti$_3$C$_2$T$_x$ (T=O, OH)	9.1 %	36.9 μg h^{-1} mg$^{-1}_{\text{cat.}}$	0.1 M HCl	-0.3 V	J. Mater. Chem. A, 2019,10.1039/c9ta03254a
La$_2$Ti$_2$O$_7$	4.55 %	25.15 μg h^{-1} mg$^{-1}_{\text{cat.}}$	0.1 M HCl	-0.55 V	Chem. Commun., 2019,55, 6401-6404
PTCA-rGO	6.9 %	24.7 μg h^{-1} mg$^{-1}_{\text{cat.}}$	0.1 M HCl	-0.5 V	J. Mater. Chem. A, 2019,7, 12446-12450
Vo-Ta$_2$O$_5$	8.9 %	15.9 μg h^{-1} mg$^{-1}_{\text{cat.}}$	0.1 M HCl	-0.7 V	ACS Sustain Chem.Eng. 2019, 710, 9622-9628
N-doped porous carbons	10.8 %	9.8 μg h^{-1} cm^{-2}	0.05 M H$_2$SO$_4$	-0.5 V	Adv. Mater. 2019, 31, 1805367
BiVO$_4$	10.04 %	8.6 μg h^{-1} cm^{-2}	0.2 M Na$_2$SO$_4$	-0.5 V	Small Methods 2018, 1800333
O-MWCNT	**3.71 %**	**9.8 μg h^{-1} mg$^{-1}_{\text{cat.}}$**	**0.1 M HCl**	**-0.3 V**	**This work**
FePc/O-MWCNT	**9.73 %**	**36 μg h^{-1} mg$^{-1}_{\text{cat.}}$**	**0.1 M HCl**	**-0.3 V**	**This work**

Reference:

[1] M. J. Frisch, G. W. Trucks, H. B. Schlegel, G. E. Scuseria, M. A. Robb, J. R. Cheeseman, G. Scalmani, V. Barone, G. A. Petersson, H. Nakatsuji, X. Li, M. Caricato, A. V. Marenich, J. Bloino, B. G. Janesko, R. Gomperts, B. Mennucci, H. P. Hratchian, J. V. Ortiz, A. F. Izmaylov, J. L. Sonnenberg, D. Williams-Young, F. Ding, F. Lipparini, F. Egidi, J. Goings, B. Peng, A. Petrone, T. Henderson, D. Ranasinghe, V. G. Zakrzewski, J. Gao, N. Rega, G. Zheng, W. Liang, M. Hada, M. Ehara, K. Toyota, R. Fukuda, J. Hasegawa, M. Ishida, T. Nakajima, Y. Honda, O. Kitao, H. Nakai, T. Vreven, K. Throssell, J. A. Montgomery, Jr., J. E. Peralta, F. Ogliaro, M. J. Bearpark, J. J. Heyd, E. N. Brothers, K. N. Kudin, V. N. Staroverov, T. A. Keith, R. Kobayashi, J. Normand, K. Raghavachari, A. P. Rendell, J. C. Burant, S. S. Iyengar, J. Tomasi, M. Cossi, J. M. Millam, M. Klene, C. Adamo, R. Cammi, J. W. Ochterski, R. L. Martin, K. Morokuma, O. Farkas, J. B. Foresman, and D. J. Fox, Gaussian 16, Revision B.01, Gaussian, Inc., Wallingford CT, 2016.

[2] Y. Zhao, D. G. Truhlar, The M06 suite of density functionals for main group thermochemistry, thermochemical kinetics, noncovalent interactions, excited states, and transition elements: two new functionals and systematic testing of four M06-class functionals and 12 other functionals. Theor. Chem. Acc., 2008, 120, 215-241.

[3] F. Weigend, R. Ahlrichs. Balanced basis sets of split valence, triple zeta valence and quadruple zeta valence quality for H to Rn: Design and assessment of accuracy. Phys. Chem. Chem. Phys., 2005, 7, 3297-3305.

[4] I. Mayer. Charge, bond order and valence in the AB initio SCF theory. Chem. Phys. Lett., 1983, 97, 270-274.

[5] T. Lu, F. Chen. Multiwfn: A multifunctional wavefunction analyzer. J. Comput. Chem., 2012, 33, 580-592.

[6] E. Skulason, T. Bligaard, S. Gudmundsdóttir, F. Studt, J. Rossmeisl, F. Abild-Pedersen, T. Vegge, H. Jónsson, J. K. Nørskov. A theoretical evaluation of possible transition metal electro-catalysts for N_2 reduction. Phys. Chem. Chem. Phys., 2012, 14, 1235-1245.

[7] J. Zhao, Z. Chen. Single Mo atom supported on defective boron nitride monolayer as an efficient electrocatalyst for nitrogen fixation: a computational study. J. Am. Chem. Soc., 2017, 139, 12480-12487.